Journal of Materials Chemistry A 7.39 (2019): 22475-22486
DOI: https://doi.org/10.1039/C9TA06072C

Electronic Supplementary Information

Liquid Phase Exfoliation of Antimonene: Systematic Optimization, Characterization and Electrocatalytic Properties

Carlos Gibaja [a,†], Mhamed Assebban [b,c,†], Iñigo Torres [a,†], Michael Fickert, [b] Roger Sanchis-Gual [c], Isaac Brotons [c], Juan José Palacios [d,e], Enrique García Michel [d,e], Gonzalo Abellán [b,c,], Félix Zamora [a,e,g*]*

[a]*Departmento de Química Inorgánica and Institute for Advanced Research in Chemical Sciences (IAdChem), Universidad Autónoma de Madrid, 28049, Madrid, Spain.*

[b]*Instituto de Ciencia Molecular (ICMol), Universidad de Valencia, Catedrático José Beltrán 2, 46980, Paterna, Valencia, Spain.*

[c]*Department of Chemistry and Pharmacy & Joint Institute of Advanced Materials and Processes (ZMP), Friedrich-Alexander-Universität Erlangen-Nürnberg (FAU), Dr.-Mack-Straße 81, 90762, Fürth, Germany.*

[d]*Instituto de Física, Universidade Federal do Rio de Janeiro, Caixa Postal 68528, Rio de Janeiro, RJ 21941-972, Brazil.*

[e]*Departamento de Física de la Materia Condensada Universidad Autónoma de Madrid, 28049 Madrid, Spain.*

[f]*Condensed Matter Physics Center (IFIMAC) Universidad Autónoma de Madrid, 28049 Madrid, Spain.*

[g]*Instituto Madrileño de Estudios Avanzados en Nanociencia (IMDEA-Nanociencia), Cantoblanco, Madrid E-28049, Spain.*

SI.1 Solvent Selection

It is well-known that successful LPE solvents have surface tension within a well-defined range.[1,2,3] Therefore, the concentration of the suspension is maximized when the energy cost of the exfoliation process is minimized, *i.e.* when the surface energy of the solvent matches with the surface energy of the layered crystals, as shown in eq. (1).

$$\frac{\Delta H_{mix}}{V_{mix}} \approx \frac{2}{T_{layer}} \left(\delta_{layer} - \delta_{solvent}\right)^2 \emptyset \qquad \text{eq. (1)}$$

Where $\delta_i = \sqrt{E_{sur}^i}$ is the square root of the component surface energy, T_{layer} is the thickness of an antimonene flake and $\emptyset$ is the volume fraction.

We calculated a value of surface energy for antimony equal to 148.8 mJ·m^{-2} (Figure S4 and "Theoretical Surface Energy Calculations" section, see below). Obviously, this theoretical value does not consider the dynamics of the liquid-phase process, so we expect it to be reasonably higher compared to the one reported experimentally.[4] For this reason, in our initial survey we have selected solvents with a wide variety of surface tensions (the surface energy of the solvents can be calculated from $\gamma = E_{sur}^{sol} - TS_{sur}^{sol}$, using an universal value for surface entropy of ~0.1 mJ·m^{-2}·K^{-1}),[2] but intentionally we also included some solvents known to be good dispersants for layered materials (Table S1).

Every experiment was run by triplicate and the concentration values represent the mean value of the three results. Samples prepared with SDS and SC were discarded from the initial survey because we do not observe Tyndall effect in their colorless suspensions.

To choose the most suitable solvent from the initial survey, we focused at first in the final FL antimonene concentration obtained after centrifuging the samples. Figure S5a shows the values of concentration, using turbidity measurements (Figure S1), as a function of the surface tension of each solvent.

Table S1. Solvents used in the study and their surface tension (at 20 ºC).

Solvent	Surface tension (mJ/m²)	Solvent	Surface tension (mJ/m²)
IPA/H_2O (4/1)	22.62	NMP/H_2O (2/1)	44.01
IPA/H_2O (2/1)	24.1	NMP/H_2O (1/1)	45.26
IPA/H_2O (1/1)	24.25	NMP/H_2O (1/4)	48.05
IPA/H_2O (1/2)	27.92	SC/H_2O (2 g/L)	57.5
IPA/H_2O (1/4)	32.26	SC/H_2O (4 g/L)	53.1
H_2O	72.7	SC/H_2O (6 g/L)	51.24
IPA	21.15	DMF	37.1
2-Butanol	22.6	DMSO	42.9
Ethanol	22.1	Hexane	18.43
Acetone	25.2	Ethyl acetate	23.2
$CHCl_3$	27.5	PEG/H_2O (0.5%)	71.8
THF	26.4	PEG/H_2O (5%)	62.37
NMP	41.26	SDS/H_2O (0.5%)	38.3
NMP/H_2O (4/1)	42.78	SDS/H_2O (5%)	38.3

**IPA: 2-propanol, THF: Tetrahydrofuran, NMP: N-Methyl-2-pyrrolidone, SC: Sodium cholate, DMF: Dimethylformamide, DMSO: Dimethyl sulfoxide, PEG: Polyethylene glycol and SDS: Sodium dodecyl sulfate.*

First, we observe that almost all the solvents tested can disperse some amount of Sb. However, the concentration of the dispersions increases for solvents with surface tensions in the range of 23-42 $mJ \cdot m^{-2}$, what means surface energy values in the range of 52-71 $mJ \cdot m^{-2}$. These values are reasonably close to the surface energy value that we calculated for Sb (*ca.*148.8 $mJ \cdot m^{-2}$). On the other hand, it is well-known that surface energy calculations overestimate the surface energy of layered materials due to the assumptions of ideality in a heterogeneous process, what is our case. This could be easily seen in the large spread of surface energy values for graphite reported in bibliography.[5,6]

Even though the analysis of the suspension concentration as a function of the surface tension is a good starting point, there is an evident problem with the data from Figure S5a, many solvents are included with apparently correct surface tension value but low concentration. This issue is something commonly observed in LPE of other layered materials.[7,8] To further investigate the mechanism of the exfoliation/dispersion process, is necessary to take a look into the solute-solvents interactions, by calculating the Hansen solubility parameters (δ_H, δ_P, and δ_D), and also calculating the best well-known solubility parameter, the Hildebrand parameter (δ_T). Both group of parameters are related as shown in eq. (2).

$$\delta_T{}^2 = \delta_H{}^2 + \delta_P{}^2 + \delta_D{}^2 \qquad \text{eq. (2)}$$

Where δ_T is the Hildebrand parameter, δ_H is the H-bonding contribution, δ_P is the polar contribution and δ_D is the non-polar or dispersive contribution to the Hansen solubility parameters. We calculate these parameters for the initial survey of solvents and plotted them against the concentration values (Figure S5b-e).

If we take a look to Figure S5b, it can be easily seen that there is almost a defined peak between 22-30 $MPa^{1/2}$ for the δ_T parameter, but this result has the same problem of the surface tension, some solvents with a calculated value of δ_T within this range have low concentration. This problem could be answered saying that, as well as with the surface tension, the Hildebrand parameter is too rough to fully describe the exfoliation/dispersion process. However, we can easily observe how according to the Hansen's model, there is a defined peak for δ_D parameter close to 17 $MPa^{1/2}$, and for the other parameters it could also be found a peak between 7-22 $MPa^{1/2}$. This results clearly show that the best solvents to enhance the concentration of FL antimonene suspensions should match with this set of Hansen solubility parameters (Table S2).

Table S2. Range of Hansen solubility parameters for promising solvents to obtain FL antimonene suspensions.

Range of δ_D ($MPa^{1/2}$)	Range of δ_P ($MPa^{1/2}$)	Range of δ_H ($MPa^{1/2}$)
16-18	7-13	7-22

SI.2 Theoretical Surface Energy Calculations.

First-principles calculations within the density functional theory (DFT) formalism are carried out using the Quantum-ESPRESSO package.[9] The Perdew-Burke-Ernzerhof (PBE) functional within the generalized gradient approximation (GGA) is used.[10] For the Brillouin-zone integration, we use a Monkhorst-Pack set of special k-points.[11] A norm-conserving pseudopotential is used for Sb with electrons in a $5s^2 5p^3 4d^{10} 5d^{-1}$ configuration. The kinetic energy cutoff for the plane wave basis are 40 Ry for the wave function and 400 Ry for the charge density. Surfaces were constructed using a supercell with a thin slab of Sb(111) separated from its periodic images by a layer of vacuum. The size of this region is such that there are always ~ 20 of vacuum between the surfaces. For the Sb(111) surface a hexagonal cell with a base defined by a_0[110] and a stacking of ABCABC is used, where a_0 is the equilibrium lattice parameter.

The surface energy is defined as the energy required to create a new surface. In our calculations the surface energy can be determined by taking the energy difference between the total energy of a slab and an equivalent bulk reference amount:

$$\gamma = \frac{1}{2A}\left(E_{slab}^{total} - E_{bulk}^{ref}\right)$$

Where E_{slab}^{total} and E_{bulk}^{ref} the total energy of the slab and the total energy of the bulk reference, respectively. A is the surface unit area, and the factor 1/2 is used because the E_{slab}^{total} has two surfaces.

SI.3 XPS results and data analysis

XPS data on the samples prepared using 2-butanol and NMP appear in Figures S9 and S10, respectively. The figures show the deconvolution in different components of the same data presented in Figure 5, corresponding to the O 1*s* and Sb 3*d* region. A weak signal coming from Sb 3*d*5/2.in oxidation state zero is seen near 582.5 eV. Oxidized Sb 3*d*5/2 appears at 530.9 eV. The main O 1*s* peak is seen at 532.5 eV, and secondary peak attributed to the presence of hydroxide species appears at 534 eV.

SI.4 Figures

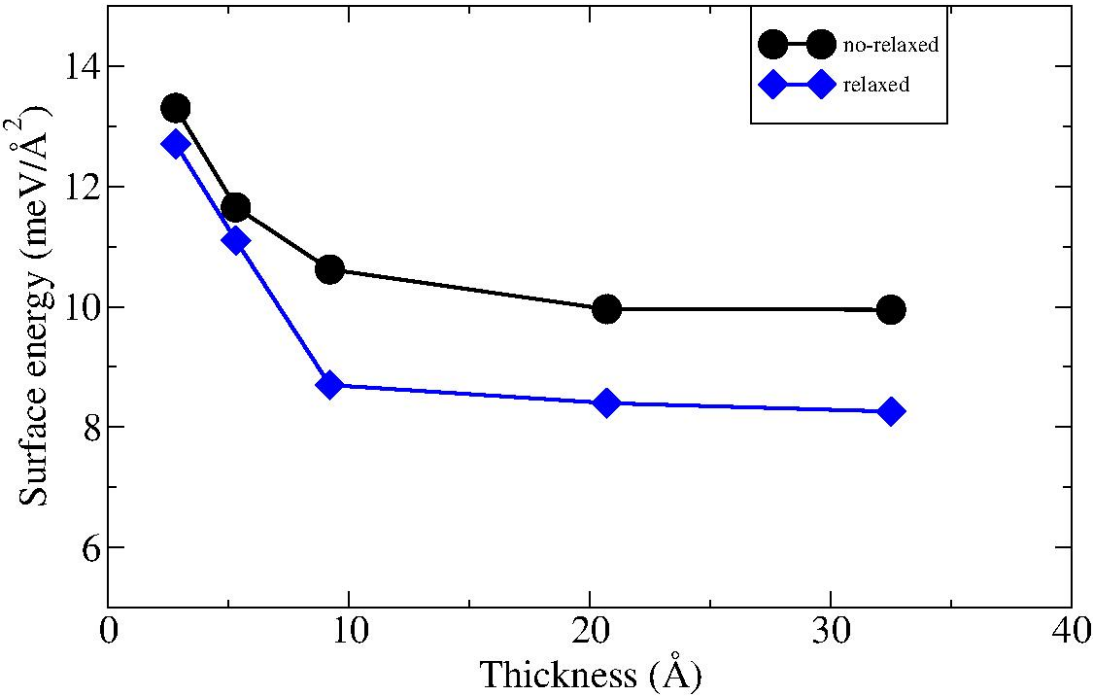

Figure S1. Calculated surface energies for Sb(111) slabs in both unrelaxed and fully relaxed geometries.

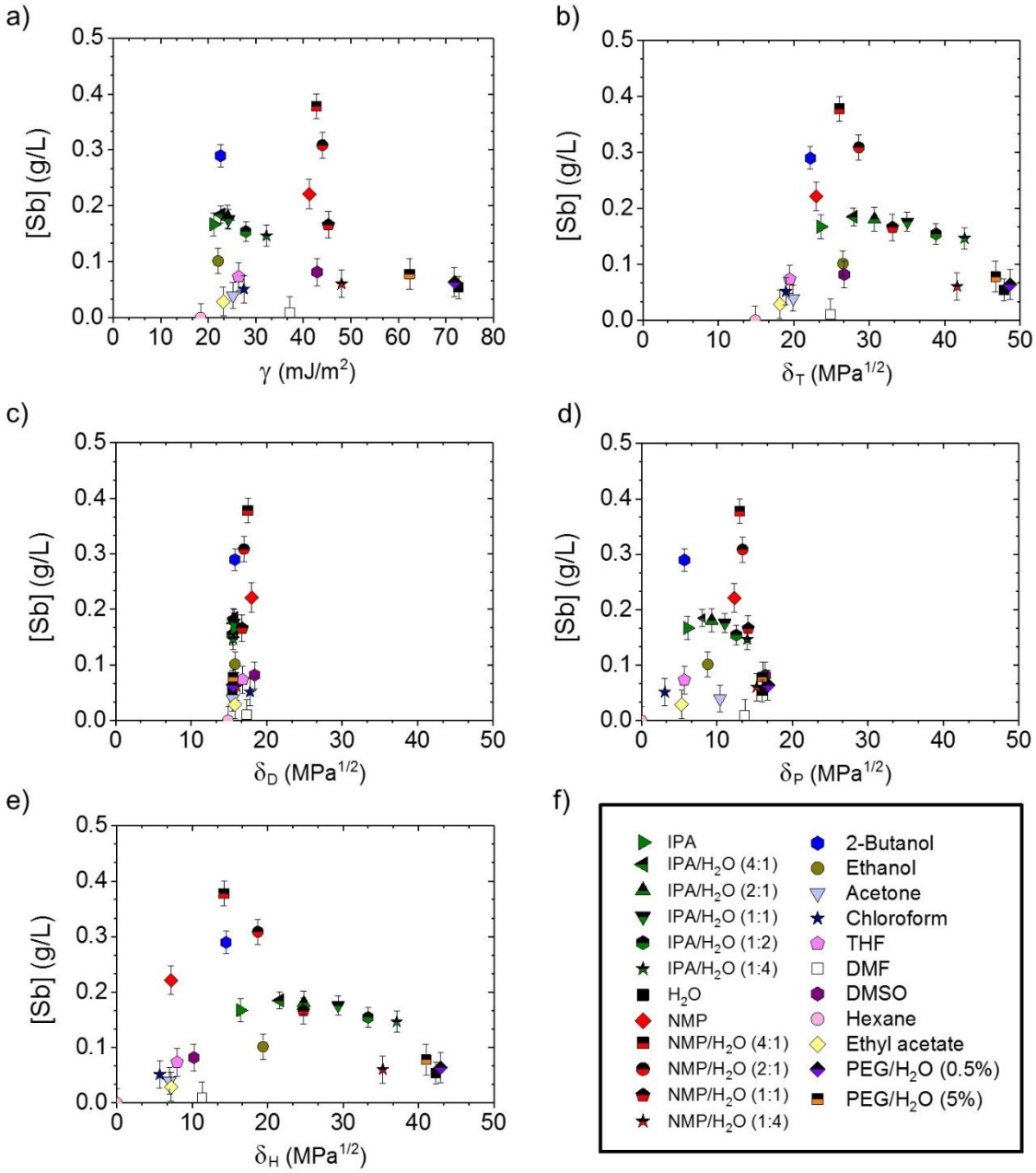

Figure S2. Concentration of FL-antimonene in suspension after tip sonication and centrifugation, [Sb] (g/L), plotted as a function of: a) surface tension of the solvents (mJ/m^2), b) Hildebrand's solubility parameter, δ_T (MPa$^{1/2}$), c) dispersive or non-polar contribution to the Hansen parameters, δ_D (MPa$^{1/2}$), d) polar contribution to the Hansen parameters, δ_P (MPa$^{1/2}$) and H-bonding contribution to the Hansen parameter, δ_H (MPa$^{1/2}$). f) legend of solvents appearing in Figure S2a-d.

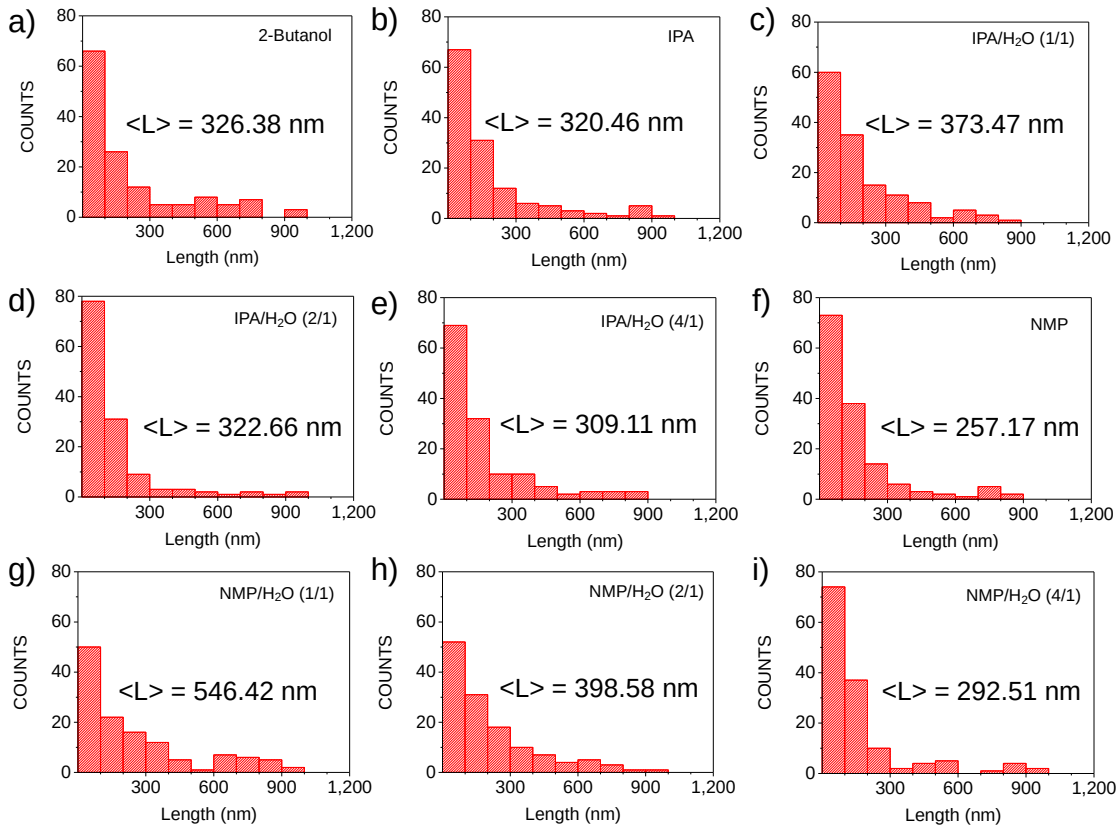

Figure S3. Length histogram of the Sb nanolayers contained in the different samples obtained using: a) 2-butanol, b) IPA, c) IPA/H_2O (1:1), d) IPA/H_2O (2:1), e) IPA/H_2O (4:1), f) NMP, g) NMP/H_2O (1:1), h) NMP/H_2O (2:1) and i) NMP/H_2O (4:1). <L> represents the mean length value in nm.

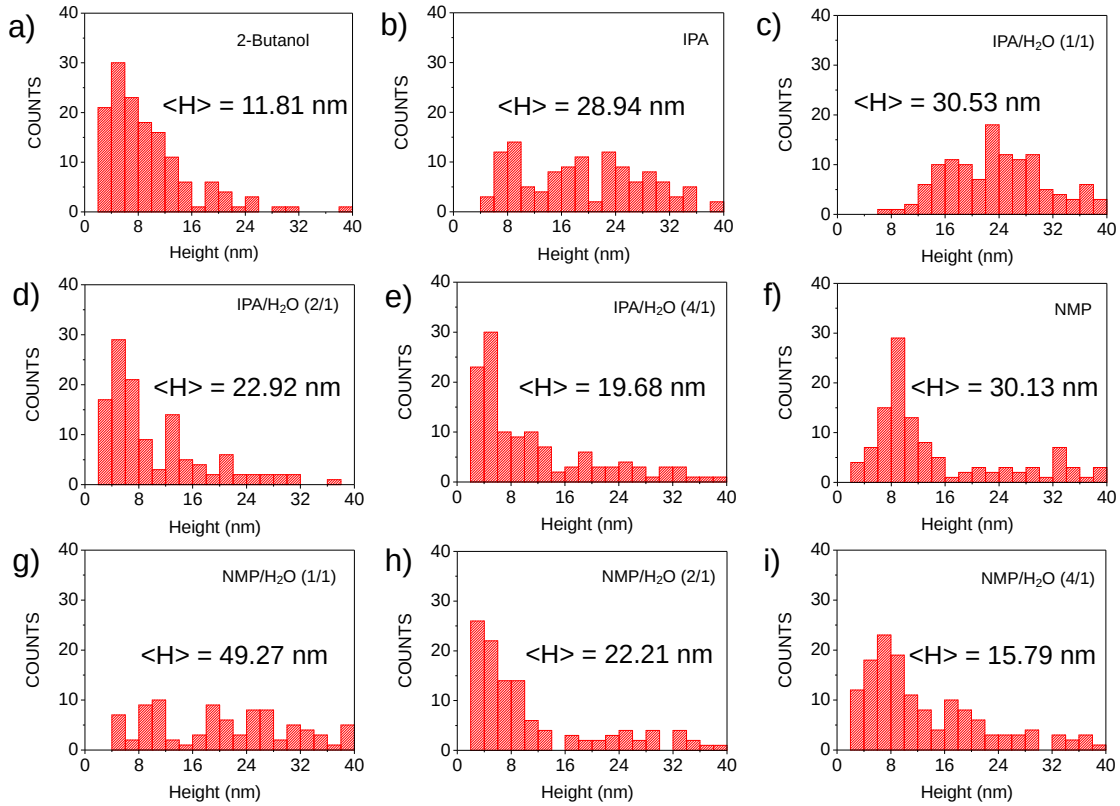

Figure S4. Height histogram of the nanolayers contained in the different samples obtained using: a) 2-butanol, b) IPA, c) IPA/H_2O (1:1), d) IPA/H_2O (2:1), e) IPA/H_2O (4:1), f) NMP, g) NMP/H_2O (1:1), h) NMP/H_2O (2:1) and i) NMP/H_2O (4:1). <H> represents the mean height value in nm.

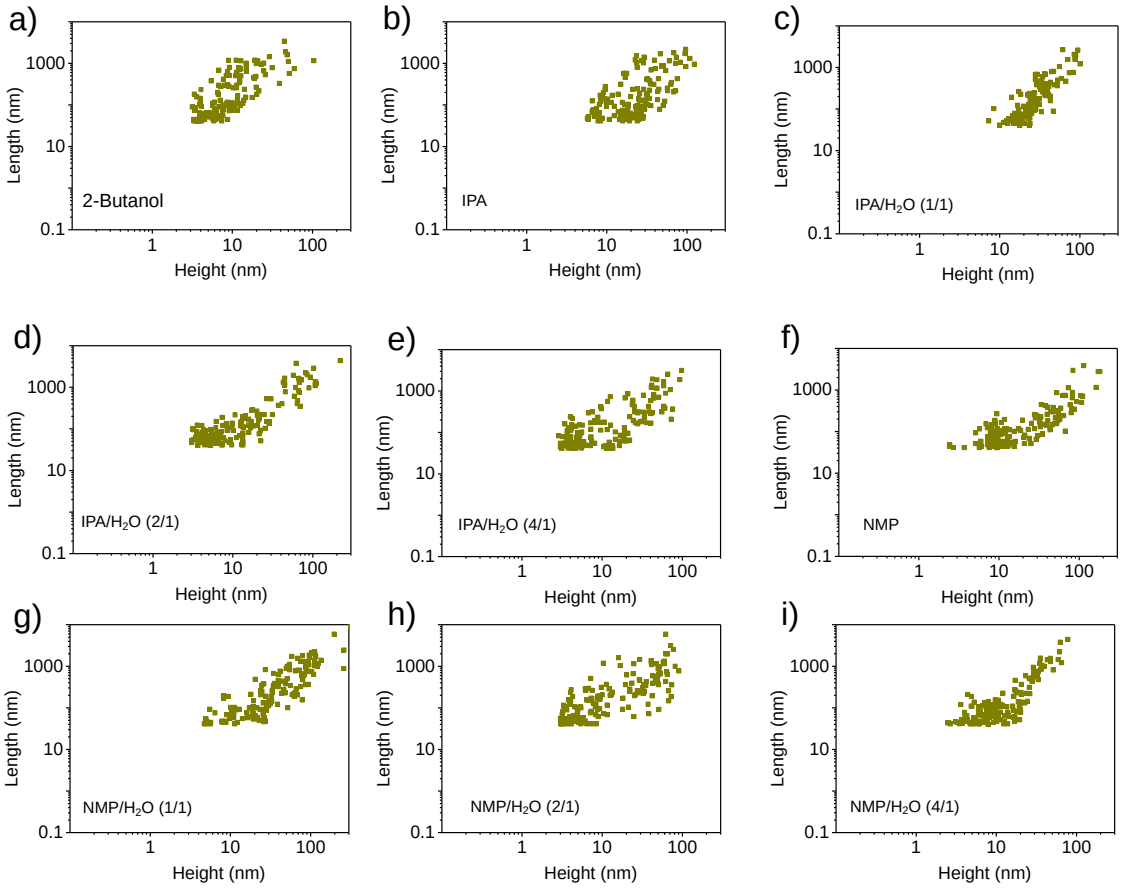

Figure S5. Plot of the length as a function of the height, of the nanolayers contained in the different samples obtained using: a) 2-butanol, b) IPA, c) IPA/H_2O (1:1), d) IPA/H_2O (2:1), e) IPA/H_2O (4:1), f) NMP, g) NMP/H_2O (1:1), h) NMP/H_2O (2:1) and i) NMP/H_2O (4:1).

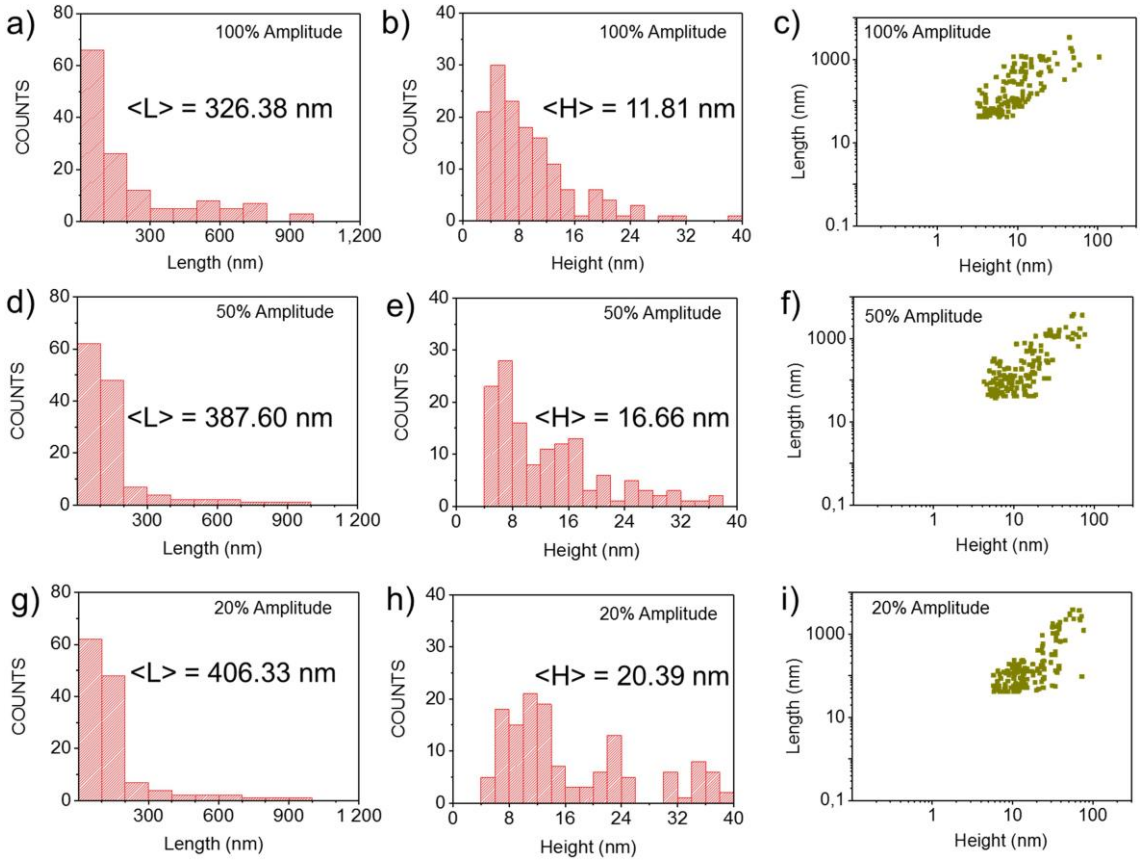

Figure S6. Height histogram, length histogram and plot of the length as a function of the height of the nanolayers contained in the samples prepared using different wave amplitudes: a), b), c) 100%, d), e), f) 50% and g), h), i) 20%.

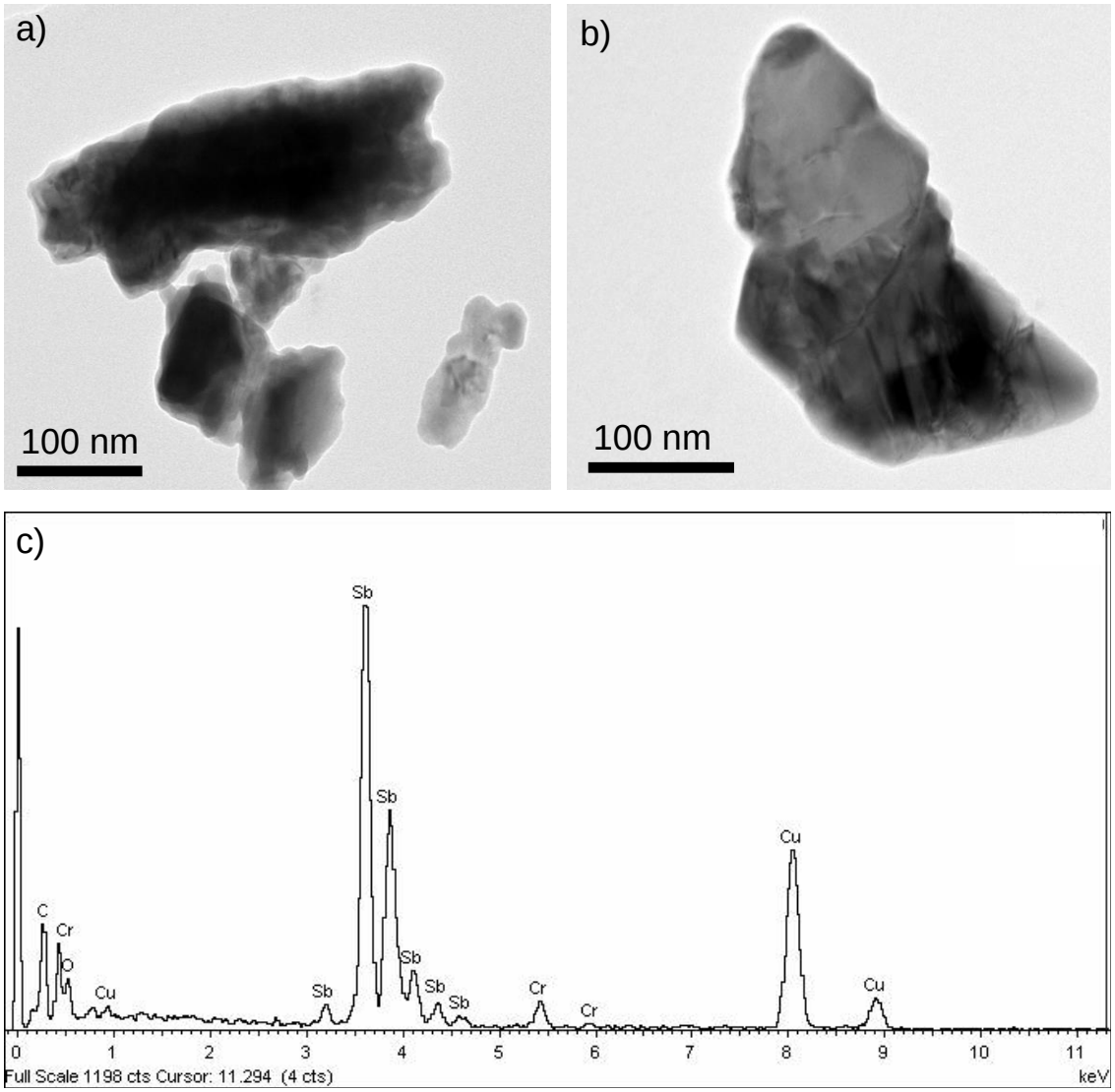

Figure S7. a), b) TEM image of FL-antimonene obtained using 2-butanol as solvent, c) X-Ray Energy Dispersive Spectroscopy (XEDS) microanalysis of FL antimonene.

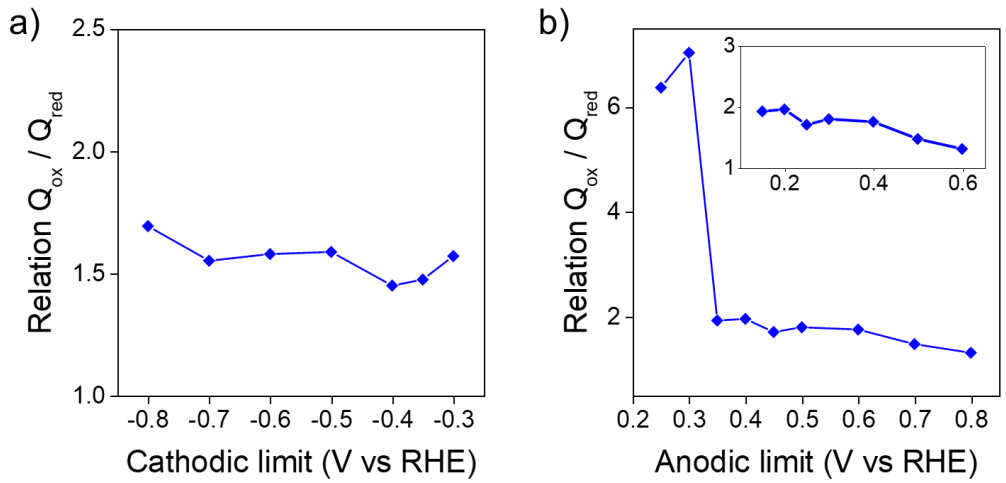

Figure S8. Charge ratio (Q_{ox}/Q_{red}) depending on the anodic limits (a) and depending on the cathodic limits (b).

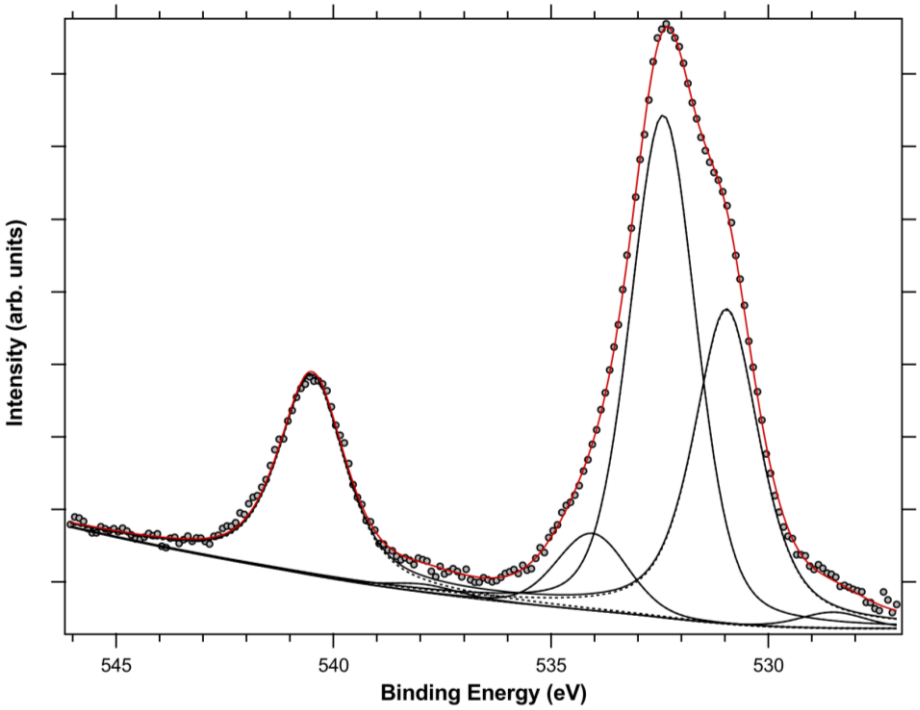

Figure S9. XPS Sb 3*d* and O 1*s* region of the FL antimonene sample prepared using 2-butanol, deconvoluted in different components (see text for identification). Dots are experimental points and the red line is the results of fit. Dashed lines correspond to the split components for 3*d* peaks ($3d_{5/2}$ and $3d_{3/2}$) and solid lines are used for the Shirley background and for the sum of the individual components of 3d peaks and the single component of 1*s* peaks.

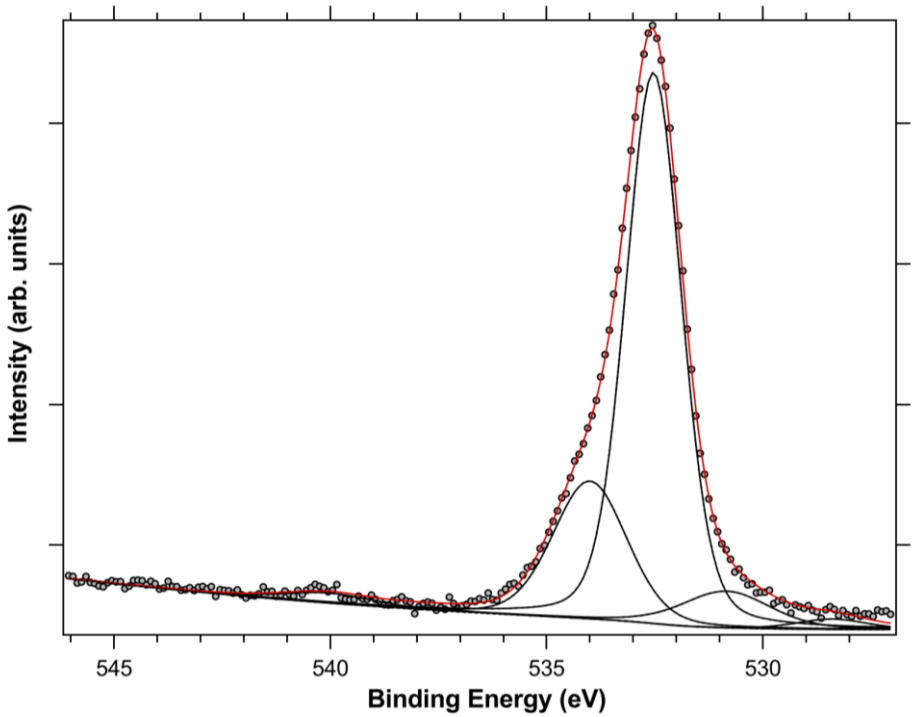

Figure S10. XPS Sb 3*d* and O 1*s* region of the FL antimonene samples prepared using NMP, deconvoluted in different components (see text for identification). Dots are experimental points and the red line is the results of fit. Dashed lines correspond to the split components for 3*d* peaks ($3d_{5/2}$ and $3d_{3/2}$) and solid lines are used for the Shirley background and for the sum of the individual components of 3*d* peaks and the single component of 1s peaks.

References

1 J. N. Coleman, M. Lotya, A. O'Neill, S. D. Bergin, P. J. King, U. Khan, K. Young, A. Gaucher, S. De, R. J. Smith, I. V. Shvets, S. K. Arora, G. Stanton, H. Y. Kim, K. Lee, G. T. Kim, G. S. Duesberg, T. Hallam, J. J. Boland, J. J. Wang, J. F. Donegan, J. C. Grunlan, G. Moriarty, A. Shmeliov, R. J. Nicholls, J. M. Perkins, E. M. Grieveson, K. Theuwissen, D. W. McComb, P. D. Nellist and V. Nicolosi, *Science*, 2011, **331**, 568–571.

2 Y. Hernandez, V. Nicolosi, M. Lotya, F. M. Blighe, Z. Sun, S. De, I. T. McGovern, B. Holland, M. Byrne, Y. K. Gun'Ko, J. J. Boland, P. Niraj, G. Duesberg, S. Krishnamurthy, R. Goodhue, J. Hutchison, V. Scardaci, A. C. Ferrari and J. N. Coleman, *Nat. Nanotechnol.*, 2008, **3**, 563–568.

3 C. Backes, T. M. Higgins, A. Kelly, C. Boland, A. Harvey, D. Hanlon and J. N. Coleman, *Chem. Mater.*, 2017, **29**, 243–255.

4 X. Wang, J. He, B. Zhou, Y. Zhang, J. Wu, R. Hu, L. Liu, J. Song and J. Qu, *Angew. Chem., Int. Ed.*, 2018, **57**, 8668–8673.

5 L. X. Benedict, N. G. Chopra, M. L. Cohen, A. Zettl, S. G. Louie and V. H. Crespi, *Chem. Phys. Lett.*, 1998, **286**, 490–496.

6 S. D. Bergin, V. Nicolosi, P. V. Streich, S. Giordani, Z. Sun, A. H. Windle, P. Ryan, N. P. P. Niraj, Z. T. T. Wang, L. Carpenter, W. J. Blau, J. J. Boland, J. P. Hamilton and J. N. Coleman, *Adv. Mater.*, 2008, **20**, 1876–1881.

7 Y. Hernandez, M. Lotya, D. Rickard, S. D. Bergin and J. N. Coleman, *Langmuir*, 2010, **26**, 3208–3213.

8 V. Nicolosi, M. Chhowalla, M. G. Kanatzidis, M. S. Strano and J. N. Coleman, *Science*, 2013, **340**, 1226419–1226419.

9 P. Giannozzi, S. Baroni, N. Bonini, M. Calandra, R. Car, C. Cavazzoni, D. Ceresoli, G. L. Chiarotti, M. Cococcioni, I. Dabo, A. Dal Corso, S. de Gironcoli, S. Fabris, G. Fratesi, R. Gebauer, U. Gerstmann, C. Gougoussis, A. Kokalj, M. Lazzeri, L. Martin-Samos, N. Marzari, F. Mauri, R. Mazzarello, S. Paolini, A. Pasquarello, L. Paulatto, C. Sbraccia, S. Scandolo, G. Sclauzero, A. P. Seitsonen, A. Smogunov, P. Umari and R. M. Wentzcovitch, *J. Phys. Condens. Matter*, 2009, **21**, 395502.

10 J. P. Perdew, K. Burke and M. Ernzerhof, *Phys. Rev. Lett.*, 1996, **77**, 3865–3868.

11 H. J. Monkhorst and J. D. Pack, *Phys. Rev. B*, 1976, **13**, 5188–5192.